ELSEVIER

ISPRS Journal of Photogrammetry & Remote Sensing 57 (2002) 39–52

PHOTOGRAMMETRY & REMOTE SENSING

www.elsevier.com/locate/isprsjprs

Monitoring high-mountain terrain deformation from repeated air- and spaceborne optical data: examples using digital aerial imagery and ASTER data

Andreas Kääb*

Department of Geography, University of Zurich, Winterthurerstrasse 190, 8057 Zurich, Switzerland

Received 15 January 2002; accepted 23 August 2002

Abstract

High mountains represent one of the most dynamic environments on earth. Monitoring their terrain changes is necessary to understand mass-transport systems, to detect related environmental variability, and to assess natural hazards. Here, we apply standard software to automatically generate digital elevation models (DEM) from aerial photography and Advanced Spaceborne Thermal Emission and Reflection Radiometer (ASTER) satellite stereo imagery. By comparison to a photogrammetrically derived DEM, an accuracy of ± 60 m RMS of the ASTER DEM was found for rough high-mountain topography, and ± 18 m RMS for moderately mountainous terrain. Differences between multi-temporal DEMs are used to determine vertical terrain changes. Horizontal movements are computed from multi-temporal orthoimages. The techniques are applied for three case studies. (1) The flow-field of Tasman glacier, New Zealand, as measured from ASTER data, showed glacier speeds of up to 250 m per year and a surprising minimum speed in the middle of the glacier. (2) The velocity-field of creeping mountain permafrost in Val Muragl, Swiss Alps, with speeds of up to 0.5 m per year was determined with high resolution from aerial stereo imagery and provided new insights in the spatial coherence of permafrost creep. (3) Deformations of up to 0.1 m per year on a large landslide near Aletsch glacier, Swiss Alps, could be detected. As a rule of thumb, we estimate the achieved accuracy for elevation changes and horizontal displacements to approximate the size of one image pixel, i.e. 15 m for ASTER and 0.2–0.3 m for the here-used aerial photography.

Keywords: glacier; permafrost; digital photogrammetry; remote sensing; ASTER; DEM; displacement; landslide; natural hazards; mountains

1. High-mountain terrain dynamics

Mass relocation is a characteristic result of the high relief energy of mountains. High-mountain terrain dynamics are expressed not only by systems of steady transport, such as glaciers, creeping permafrost, or slow land sliding, but also by sudden events, such as ice and rock avalanches, or debris flows. In most mountainous regions of the world, these natural mass relocations impose various hazards to human life and infrastructure. For instance:

(1) Glaciers and their fluctuations are able to form lakes whose breakouts frequently cause severe floods and debris flows (e.g. Haeberli, 1983; Clague and Evans, 2000; Richardson and Rey-

* Tel.: +41-1-6355146; fax: +41-1-6356848.
E-mail address: kaeaeb@geo.unizh.ch (A. Kääb).
URL: http://www.geo.unizh.ch/~kaeaeb.

0924-2716/02/$ - see front matter © 2002 Elsevier Science B.V. All rights reserved.
PII: S0924-2716(02)00114-4

nolds, 2000; Haeberli et al., 2001; Huggel et al., 2002).

(2) Ice break-off from steep glaciers may result in catastrophic ice avalanches, sometimes even combined with snow and/or rock avalanches (e.g. Margreth and Funk, 1999; Richardson and Reynolds, 2000; Giani et al., 2001).

(3) Recent studies propose a connection between creeping mountain permafrost and an enhanced debris-flow activity (e.g. Kääb, 2000).

(4) Relief and uncovering of steep valley flanks by retreating glaciers significantly affects the stress regime of the slopes, potentially destabilizing them (e.g. Blair, 1994; Haeberli et al., 1997).

Glacier and ground ice play a crucial role in most high-mountain systems. Due to their proximity to melting conditions under terrestrial conditions, the ice-related transport systems are especially sensitive to climate change. Therefore, monitoring high-mountain terrain dynamics serves also as an important contribution to climate monitoring. The international Global Land Ice Measurements from Space (GLIMS)-initiative aims presently at compiling a global glacier inventory and tracking glacier changes over time, mainly using data from LandSat 7 ETM+ and ASTER (Kieffer, 2000). The Intergovernmental Panel on Climate Change (IPCC) recognizes glaciers as one of the priority climate indicators (McCarthy et al., 2001). In several high-mountain regions of the world ongoing climate warming markedly intensifies hazards related to glaciers and permafrost.

Due to the remoteness of high mountains and due to the spatial extension of most mass-relocation processes, remote sensing is a prior tool for monitoring high-mountain terrain dynamics. Remote sensing and photogrammetry is able to provide data on terrain geometry, terrain cover, and three-dimensional terrain displacements. Measuring terrain deformation, i.e. vertical and horizontal displacements on the surface, significantly contributes to modeling of the dynamic processes, to understanding their sensitivities, and to early recognition of potential impacts on human and natural systems. Recent digital image analysis techniques have even enhanced the applicability of remote sensing for the above monitoring work.

In this contribution, we assess the potential and the restrictions of repeated optical air- and spaceborne imagery for digitally measuring high-mountain terrain deformation. As an example for spaceborne imagery we use ASTER data. First, we give an overview of the analysis methods applied, both using aerial photographs and data of the new ASTER satellite sensor (Section 2). Three case studies are used to assess the presented methods: glacier flow (Section 3), permafrost creep (Section 4), and landslides (Section 5).

2. Methods

A universal set of optical techniques suitable for determining geometric terrain changes under a range of conditions has necessarily to consider both satellite data and aerial (or terrestrial) imagery. Aero-photogrammetric methods are highly accurate, but the required photography is partially not available for remote regions. Often it covers only small terrain sections. On the other hand, satellite imagery is able to cover large areas by a, however, lower resolution. Combining both data sources is most promising, for instance for hazard detection where a downscaling approach from rough but area-wide assessments (i.e. the satellite domain) towards detailed investigations for small areas (i.e. the aero-photogrammetry domain) is necessary. For the satellite image analyses, we focus on data of the new Advanced Spaceborne Thermal Emission and Reflection Radiometer (ASTER, on board TERRA) as a representative for medium-resolution stereo imagery from space.

2.1. ASTER data

Deriving digital elevation models (DEM) from satellite stereo imagery is no new approach. Especially multi-temporal SPOT data from different pointing-angles have been widely used for DEM generation over mountainous terrain (e.g. Al-Rousan and Petrie, 1998; Zomer et al., 2002). One major problem, thereby, consists in the time lapse between the used images, which leads under high-mountain conditions usually to different snow and cloud cover on the stereo images. These difficulties are overcome by along-track stereo channels, such as available from ASTER.

Concerning optical satellite data, horizontal displacements on glaciers have been measured mostly from repeated LandSat or SPOT data using different

correlation techniques (e.g. Lucchitta and Ferguson, 1986; Scambos et al., 1992; Frezzotti et al., 1998; Seko et al., 1998; Nakawo et al., 1999; cf. also Van Puymbroeck et al. 2000). For such work, the spatial resolution of the used images is, besides the time period between the acquisitions, the most crucial parameter. Unique surface features, usually crevasses or debris cover, have to be identified from the available resolution. Together with sensors of similar resolution (for instance SPOT, IRS, or JERS) ASTER provides advantages also in the latter context compared to LandSat.

ASTER's spectral and geometric properties include three bands in VNIR with 15 m resolution, six bands in SWIR with 30 m, five bands in TIR with 90 m, and a 15-m resolution NIR along-track stereo-band looking back 27.6° from nadir. The stereo band 3B covers the same spectral range of 0.76–0.86 μm as the nadir band 3N. The TERRA orbits are similar to LandSat orbits (705 km altitude). ASTER swath width is approximately 60 km (180 km for LandSat). The ASTER VNIR sensor, applied in this contribution, consists of a push broom sensor of 4100 detectors (5000 for 3B) with a FOV of 6.09° (5.19° for 3B) and an IFOV of 21.5 μrad (18.6 μrad for 3B). ASTER VNIR camera constant is approximately 330 mm, scale is approximately 1:2 Mio. To cover the full range between the tracks, ASTER can be pointed ±8.5° (i.e. ±106 km) across-track (ERSDAC, 1999a,b).

For generating DEMs from ASTER data, we either use level 1B data (already corrected for striping and with band-to-band co-registration), or raw level 1A data which we destripe using the respective parameters provided by the image header information. Orientation of the 3N and according 3B band from ground control points (GCP), transformation to epipolar geometry, parallax-matching, and parallax-to-DEM conversion is done using the software PCI Geomatica 8.0 Orthoengine (Toutin and Cheng, 2001).

In areas with no sufficient ground control available, we compute such information directly from the given satellite position and rotation angles. The line-of-sight for an individual image point is intersected with the earth ellipsoid. The actual ellipsoidic elevation of a point is then estimated from the parallax between the respective point projections in 3N and 3B. Using this elevation and the spacecraft position, we correct the ellipsoidic point coordinates for their horizontal shift due to point elevation. The accuracy for this procedure is mainly influenced by the pointing and position accuracy of the spacecraft (in the order of 10^2 m) and by the parallax accuracy (one to two pixels). For this study, we did not perform an according detailed accuracy assessment for the procedure, since for determining terrain deformations the relative accuracy between the repeated data sets is more important than the absolute position of the study site (cf. below for deformation measurement). Absolute positional errors from the above procedure can be corrected to a large extent if a few GCPs are available in the study site. The GCPs obtained from above procedure or already available are imported into PCI Geomatica for bundle adjustment.

Fig. 1 shows an ASTER DEM (right) compared to a reference-DEM with 25 m spacing derived directly from 1:30,000 scale aerial photography by manual analytical photogrammetry (left; Kääb, 2001). The depicted test area Gruben in the Swiss Alps represents difficult high-mountain conditions with high relief (2000–4000 m a.s.l.), steep rock walls, deep shadows, and snowfields without contrast. Therefore, we consider the test area to represent a worst-case scenario for DEM generation from ASTER data.

Visual inspection and quantitative analysis show that severe errors of the ASTER DEM of up to approximately 500 m occur for sharp peaks with steep northern slopes. These errors are not surprising keeping in mind that such northern slopes are heavily distorted (or even totally hidden) in the 27.6° back-looking band 3B, and lie, at the same time, in shadow. However, the magnitude of the above severe errors might rather point to the weakness of the applied blunder detection algorithms within PCI Geomatica Orthoengine 8.0 than to a general characteristic of ASTER DEMs. The overall accuracy obtained for the ASTER DEM compared to the manually measured photogrammetric reference DEM amounts to ±60 m RMS. For a subsection with moderate topography (Fig. 1), but still representing typical high-mountain terrain, an accuracy of ±18 m RMS and maximum errors of 95 m were found. The latter maximum errors occur at sharp moraine ridges or deep stream channels.

Orthorectification of the ASTER imagery is computed from the obtained ASTER DEMs, again within

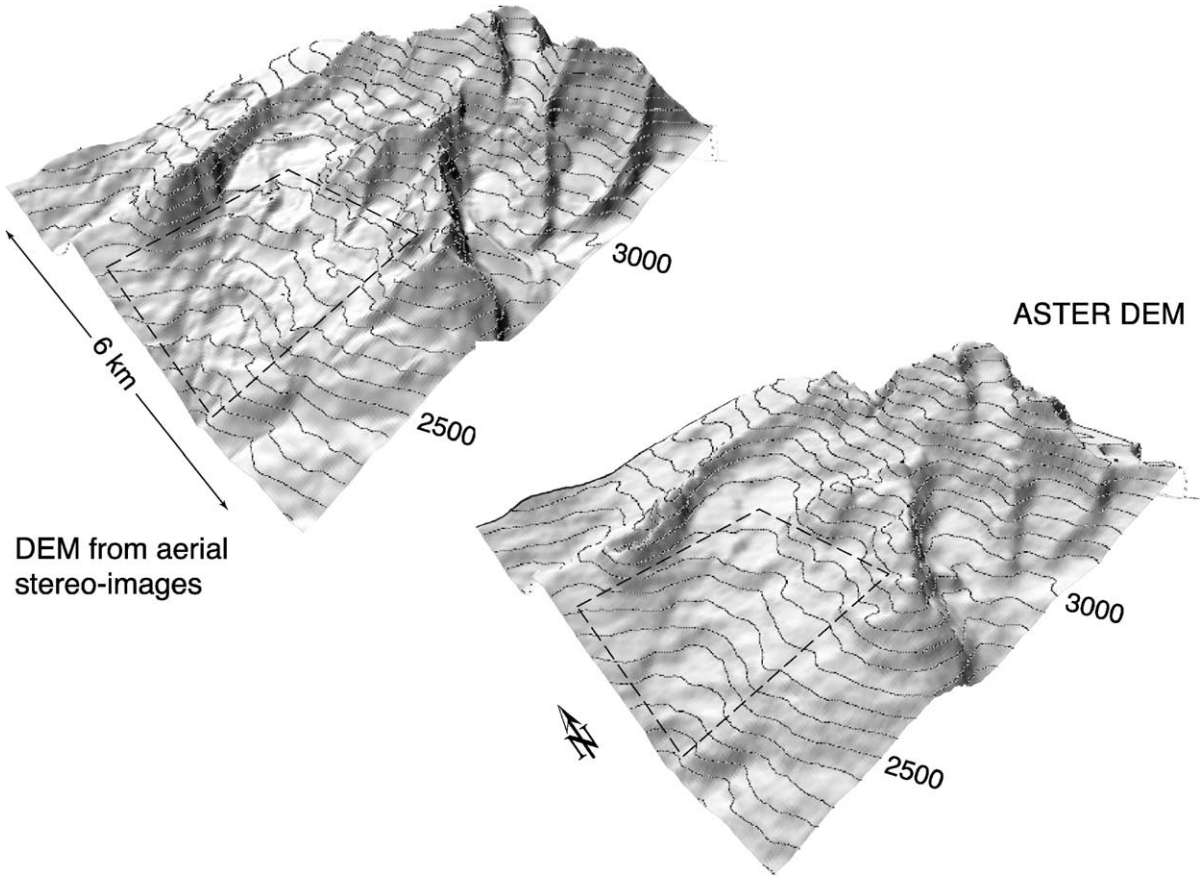

Fig. 1. Comparison between a DEM measured by analytical photogrammetry (left) and a DEM automatically computed from ASTER satellite stereo-imagery (right) for typical high-mountain terrain at Gruben, Swiss Alps (7°58′E, 46°10′N). Largest errors of the ASTER DEM occur at sharp peaks with their northern flanks hidden in the back-looking stereo channel. In total, the accuracy of the ASTER DEM was found to approximate ±60 m RMS, and ±18 m RMS for a subsection representing more moderate high-mountain terrain (rectangle).

PCI Geomatica Orthoengine. Thereby, the above estimated maximum elevation error of 500 m for extreme topography translates into a horizontal position error for the orthoprojection of approximately 90 m for the maximum 8.5° across-track pointing, the above average error of 60 m RMS translates to 10-m position error. For more moderate terrain, the position errors equivalent to the above height error of 95 or 18 m RMS, respectively, total of 17 or 3 m, respectively, for the maximum 8.5° pointing. In conclusion, from DEM errors alone an approximate position error of up to the ASTER VNIR pixel size of 15 m (or less, depending on the across-track pointing angle) has to be expected in the orthoimages for typical glacier surfaces which correspond roughly to the above moderate terrain type. (Remark: the ASTER VNIR, but not the SWIR and TIR sensors, can be pointed by ±24°. We do not use imagery pointed more than 8.5° because of the strong distortions, and because our terrain studies are usually combined with multispectral analysis applying also the SWIR and TIR bands.)

Multi-temporal orthoimages obtained from repeated ASTER imagery are applied for measuring terrain displacements. In order to avoid distortions between the multi-temporal products, all imageries (i.e. 3N and 3B of time 1, and 3N and 3B of time 2) are adjusted as one image block connected by tie-points, before orthoimage generation is performed. The tie-points for the multi-temporal model connection have to be placed on

stable terrain. For details, see Kääb (2000). The displacement for individual pixels, or surface features, respectively, between the multi-temporal satellite orthoimages is determined using double cross-correlation (Fig. 2; Kääb and Vollmer, 2000). In order to obtain some sub-pixel accuracy for the final matching, the final level of the used image pyramid is computed from cubic interpolation of the original image into a higher resolution (usually 1/2 of the original resolution). Matching blunders are detected (and eliminated) from small correlation coefficients and from applying geometric constraints such as expected flow speed and direction. Using the orthoimage georeference, the resulting displacement-parallaxes can be directly transformed into horizontal terrain displacements. Taking into account the fuzzy nature of most high-mountain terrain features, as well as considering terrain changes between the acquisition times, an overall accuracy of approximately a half to one pixel size (i.e. 7–15 m) can be expected for the horizontal displacement measurements. This accuracy estimate is derived from tests with aerial imagery (Kääb and Vollmer, 2000) and from the noise within the displacement field on a—usually coherently deforming—glacier. It is important to note that the accuracy of such image analysis is mainly restricted by terrain properties rather than by the precision of the applied algorithms. Thus, further (possible!) refinement of the here-applied procedure will, in our view, not necessarily lead to a more accurate determination of the actual terrain deformation.

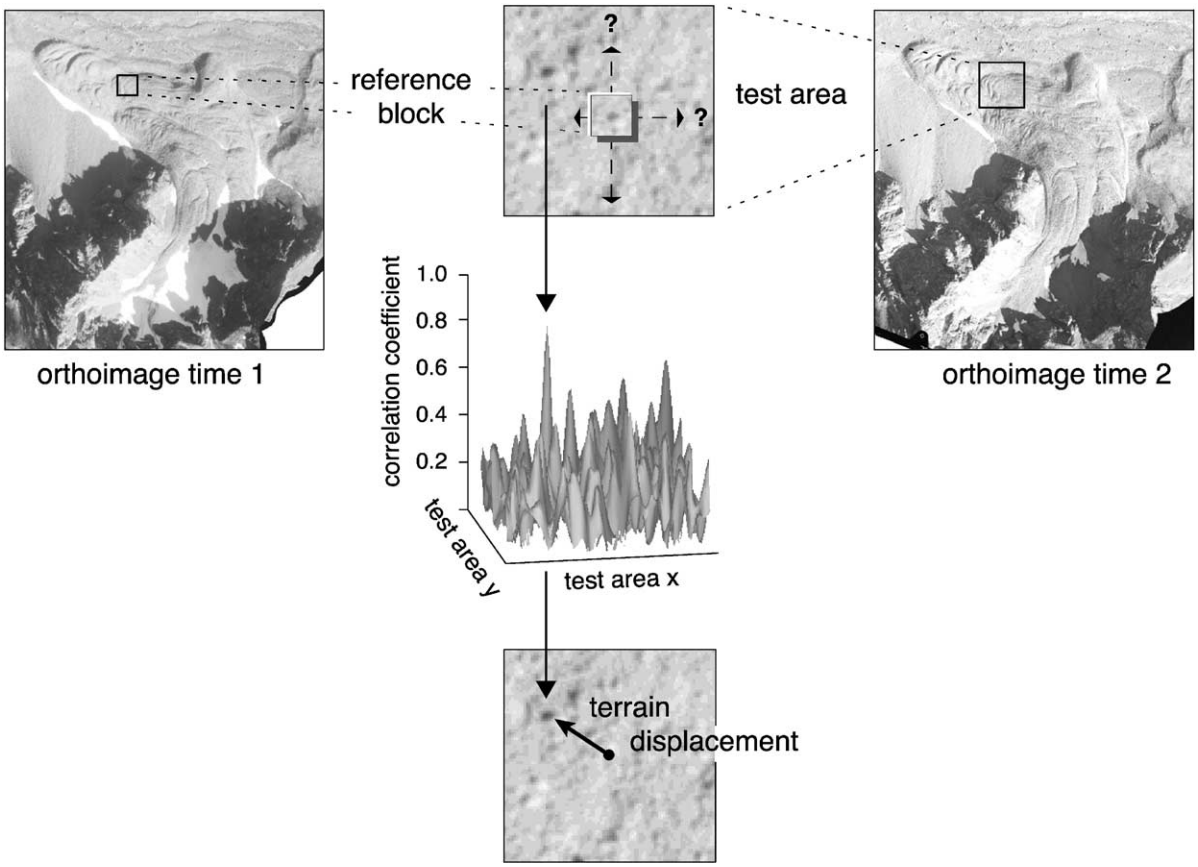

Fig. 2. Scheme of measuring surface displacements from repeated digital orthoimages by block-correlation techniques. A reference-block in the orthoimage at time 1 is searched for in a test area in the orthoimage at time 2. Applying the orthoimage georeference, the horizontal shift between the reference-block location and the corresponding test block directly gives the horizontal surface displacement.

2.2. Digital aerial photography

For detailed high-precision studies on high-mountain terrain deformation, we apply digitized aerial stereo-photography with scales ranging from 1:6000 to 1:30,000. All imageries used for the case studies below have been taken by the Swiss Federal Office of Topography/Flight service. The photographs were scanned with 30-μm resolution. Automatic DEM generation is done using standard methods of digital photogrammetry, established also for high-mountain terrain (e.g. Baltsavias et al., 1996, 2001; Würländer and Eder, 1998; Kääb and Vollmer, 2000; Kaufmann and Ladstädter, 2000). Here, DEMs and orthoimages are computed within SOCET SET of LH Systems. Similar to the above DEM-generation from ASTER data, we roughly estimate the overall accuracy of the DEMs obtained from aerial stereo-photography to lie in range of one pixel size (RMS) for high-mountain terrain (Kääb and Vollmer, 2000). Severe blunders, as usually found for steep flanks and peaks, are more seldom for the here-investigated moderate terrain type like glacier and rock glacier surfaces. However, the above accuracy estimate does not apply for terrain with little or no optical contrast such as snow cover. Changes in elevation, i.e. thickness changes of the observed terrain, are derived as differences between multi-temporal DEMs. Remarks specific to the application and analysis of analytical and digital photogrammetry for high mountains are also given in Kääb et al. (1997), Kääb and Funk (1999), and Kääb (2001).

As demonstrated by earlier studies, photogrammetry based on repeated aerial photography represents a powerful tool to measure terrain displacements in high mountains. The techniques used to date range from manual or analog comparison of repeated images, analytical point-by-point measurements, analytical simultaneous comparison, to fully digital deformation measurements (Kääb and Vollmer, 2000; Kaufmann and Ladstädter, 2000). In general, digital techniques have proven to be both highly precise and fast. Here, terrain displacements are measured from multi-temporal orthoimages applying the software Correlation Image Analysis (CIAS; Vollmer, 1999) described above for the ASTER orthoimages (Fig. 2). In order to avoid distortions between the multi-temporal products, all imageries are adjusted as one image block completely connected by tie-points. The obtained accuracy, estimated to approximately one pixel size RMS (here: 0.2–0.3 m for the 1:7000–10,000 scale imagery applied in Sections 4 and 5), is, however, governed to a large extent by the terrain conditions and their changes between the image acquisitions.

3. Glacier flow

Glacier ice deforms under the force of gravity and is able to slide on the ground. The resulting ice flow observed at the surface represents the mass transport between areas with predominant snow accumulation and those with prevailing mass loss by ice melt or break-off. Thus, measuring glacier flow-fields decisively contributes to understanding glaciers and related hazards.

Fig. 3 depicts the surface displacements between 2000 and 2001 for Tasman Glacier, New Zealand. The displacement vectors have been measured automatically from ASTER data of 29 April 2000 and 7 April 2001 using the software CIAS. The fact that one of the ASTER images was acquired in nadir mode, the other with 8.5° across-track pointing led to some low-frequency distortions in between the orthoimages, presumably from errors in exterior orientation. In order to avoid these distortions, the displacements were derived section-wise. For the individual sections, planimetric orthoimage-to-orthoimage transformations were determined from apparently stable terrain points. The parameters of the section-wise transformations were applied to correct the raw displacement vectors. In Fig. 3, the original 100-m grid of measurements is resampled to a 200-m grid for better visibility. A threshold for individual correlation coefficients to be accepted was applied and few obvious mismatches were deleted manually. Besides these procedures, Fig. 3 depicts the raw measurements. The automatic measurements did more-or-less not succeed for clean ice because the images showed no corresponding features between the two acquisition times. Especially for the upper glacier parts in April 2000, the ice was snow-covered. On debris-covered ice, however, the results look promising.

In the upper part of the glacier, ice speeds of up to 230 m year^{-1} were observed, continuously decreas-

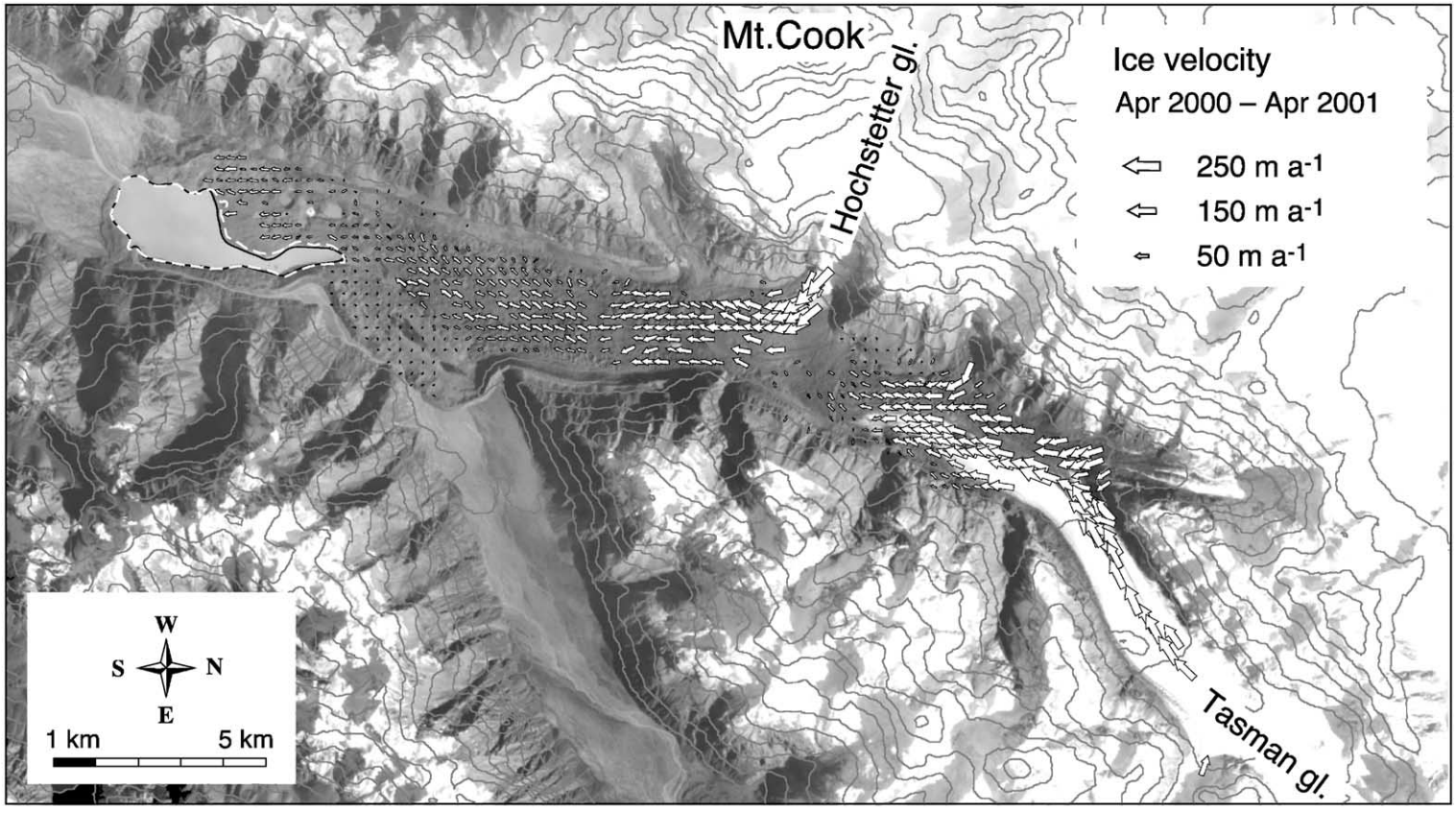

Fig. 3. Ice flow vectors for Tasman glacier, New Zealand (170°10′E, 43°35′S) derived from ASTER images of 29 April 2000 and 7 April 2001. The original 100-m spacing of the raw measurements is resampled to 200-m spacing. Ice speeds amount up to 250 m year^{-1}. The marked—and surprising—decrease of ice flow for Tasman glacier at the confluence with Hochstetter glacier indicates a complex interaction between both glaciers. At the glacier terminus lake, a dashed line marks the lake extent of 7 April 2001 superimposed on the 29 April 2000 orthoimage. The observed lake growth towards the ice front amounts up to 130 m.

ing to the central part of the depicted image section where velocities are below the significance level of approximately one pixel size (15 m). Thereby, the marked ice inflow with 250 m year^{-1} (or even more) from the western tributary Hochstetter glacier might play an important role. Below this glacier confluence, velocities decrease again towards the lake at the glacier front. To the northeast of the lake, an area with very low or even zero velocities can be recognized, presumably consisting of ice-free moraine or stable dead-ice, decoupled from the glacier.

The ice velocities measured from the ASTER data can be compared to some terrestrial and photogrammetric velocity measurements available for Tasman glacier (Kirkbride, 1995). For the lowermost 2–3 km of the glacier terminus, the velocities observed from ASTER data seem to be similar within the measurement accuracy to those observed for 1971–1986 and 1957–1971. Terrestrial velocity measurements for May to December 1986 at a region ca. 8 km upwards of the front gave 90 m year^{-1}. Velocities at the same place from ASTER data approximate 50 m year^{-1} for April 2000 to April 2001. The variations for the 8-km section indicate a marked difference in ice speed. It is not clear if this is, in fact, due to a general change in ice flow regime or just due to seasonal velocity variations. Note that the terrestrial surveying of 1986 and the ASTER measurements cover different fractions of a year.

During April 2000–April 2001, the glacier front retreated by up to 130 m at the lake (Fig. 3). The measured flow field and retreat rates of Tasman glacier are able to contribute to forecasting of the evolution of the pro-glacial lake (Kirkbride and Warren, 1999; Purdie and Fitzharris, 1999). This lake evolution mainly consists in a balance of ice melt and break-off (calving), on the one hand, and ice supply from glacier flow, on the other hand.

4. Permafrost creep

Permafrost (i.e. underground with temperatures below 0° C all year) may contain a significant percentage of ice. In high mountains, such frozen debris is able to creep and form debris lobes similar-looking to lava streams. These slope instabilities, so-called rock glaciers, are typical for dry-cold mountain regions, and may, in cases, be involved in the disposition of debris flows (Kääb, 2000). Due to their slow surface deformation of some 0.01 m year^{-1} to some 1 m year^{-1} (both horizontally and vertically), and their size of some hundred meters in maximum, rock glaciers can hardly be monitored by optical satellite imagery. Aerial photogrammetry is, therefore, a prior tool for deriving thickness changes and horizontal displacements on rock glaciers (Kääb et al., 1997; Kääb and Vollmer, 2000; Kaufmann and Ladstädter, 2000).

The horizontal surface velocity field (Fig. 4) and the thickness changes (not depicted) between 1981 and 1994 on Muragl rock glacier, Swiss Alps, have been measured from digitised stereo imagery of approximately 1:7000 scale (Kääb and Vollmer, 2000). The comparison of the 1981 and 1994 DEMs gave surface lowerings of up to -0.5 m year^{-1} in the zones of perennial ice patches in the upper part of the rock glacier indicating massive loss of ice. For the lower part of the rock glacier, a pattern of heavings and settlements in the range of ± 0.1 m year^{-1} was observed. Over the investigated period, the frozen debris of Muragl rock glacier was creeping with average horizontal surface speeds of up to 0.5 m year^{-1} (Fig. 4). Maximum creep rates occur in the steeper middle part of the rock glacier. The flow field reveals the rock glacier to be a complex system of several flow lobes, both laterally and vertically separated (Frauenfelder and Kääb, 2000). The accuracy of the displacement measurements is estimated from comparison with terrestrial surveying and analytical photogrammetry to about ± 0.2 m RMS, or ± 0.015 m year^{-1} for the 1981–1994 period, respectively (Kääb and Vollmer, 2000). The used aerial photographs were scanned with 30-μm resolution, which approximates 0.2 m in ground scale.

For the subsection marked in Fig. 4, high-resolution displacement measurements with 3-m grid spacing have been conducted (Fig. 5). The measured surface displacements depict a sharp lateral shearing between the highly active part of the rock glacier and the low or even inactive part to the northeast margin. A further result of the high-resolution measurements, which are displayed raw and unfiltered, is the uniformity of the surface deformation. Besides, the sharp lateral shearing, no spatial high-frequency variations can be seen in the velocity field. The mass is obvi-

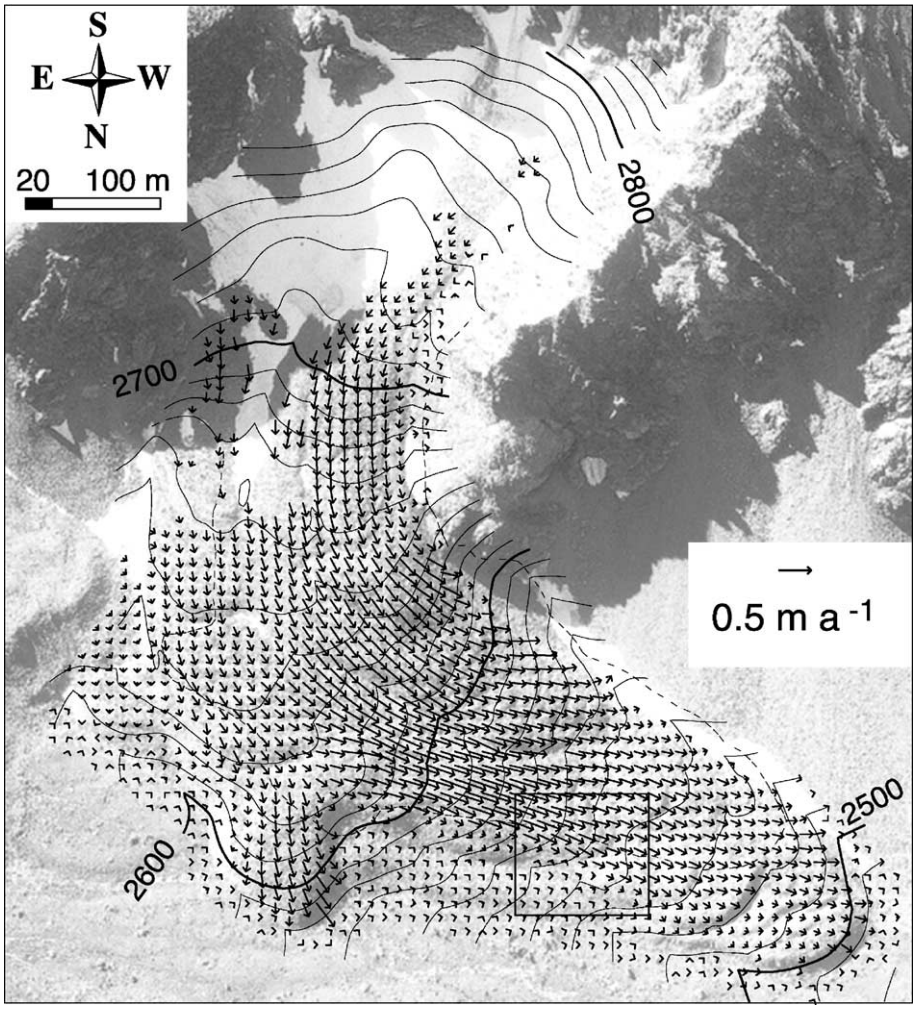

Fig. 4. Displacement vectors between 7 September 1981 and 23 August 1994 on creeping permafrost in Val Muragl, Swiss Alps (9°55.5′E, 46°30.5′N) as derived from multi-temporal orthoimage-comparison. The velocity field with speeds of up to 0.5 m year^{-1} points to a system of individual lobes separated laterally as well as vertically. The applied aerial photography was taken by the Swiss Federal Office of Topography. For the rectangle to the lower right, see Fig. 5.

ously deforming as a whole with some stress transferring material component (ice!). Measurements like the one presented here substantially increase the knowledge about the conditions and processes involved in permafrost creep, and, thus, contribute to assessing the stability of high-mountain slopes (Kääb, 2000). Since rock glaciers have been shown to be many millennia old, their investigation also helps understanding environmental change since the last ice age (Kääb et al., 1998; Haeberli et al., 1999; Frauenfelder and Kääb, 2000).

5. Landslides

In contrast to glaciers or creeping permafrost, high-mountain landslides, often deep-seated rockslides, have no significant ice content influencing their dynamics. However, many of such rockslides are closely related to glacier fluctuations. Since rockslides lack a stress-transferring medium like ice which cements individual rocks, the deformation of such slope instabilities usually is much less coherent as for rock glaciers or glaciers. Related destruction of the

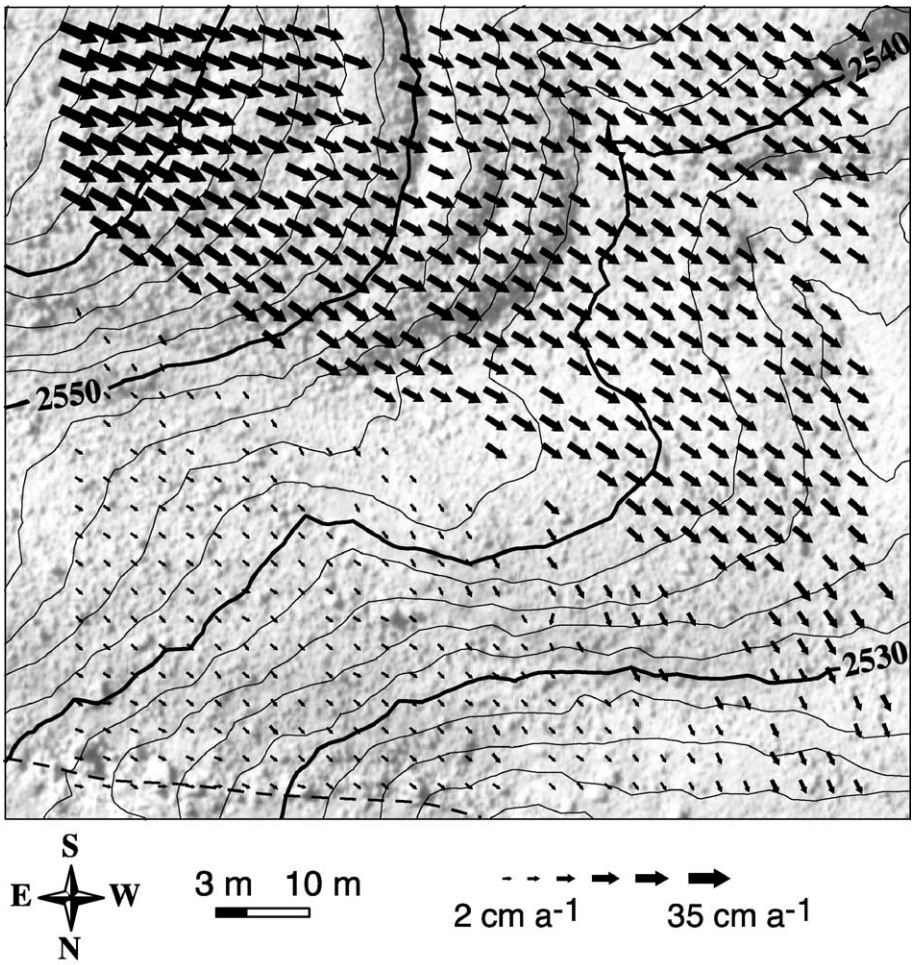

Fig. 5. Raw 3-m spaced automatic measurements of horizontal displacements for a section on the Muragl rock glacier between 1981 and 1994 (see subsection in Fig. 4). The dashed line to the North represents the margin of the rock glacier. Underlying orthoimage of 1994. The smooth velocity field indicates a highly coherent deformation over time, pointing to stress-transferring ice in the ground.

surface structure between the image acquisition times may cause problems for the direct image comparison we apply. Rockslide activity endangers surface and subsurface infrastructure, and is able to trigger other hazards, by, for instance, damming a river and causing a flood hazard. Digital image analysis techniques for mapping landslides and monitoring related elevation changes from repeated DEMs are comparably often applied (e.g. Mantovani et al., 1996; Maas and Kersten, 1997; Weber and Herrmann, 2000; Chandler, 2001), in contrast to respective horizontal displacement measurements (Mantovani et al., 1996; Powers et al., 1996; Baum et al., 1998; Kääb, 2000).

Fig. 6 shows an automatic CIAS measurement on a large rockslide at the tongue of Aletsch glacier, Swiss Alps. The displacements were derived from 1:10,000 scale aerial photography of 1976 and 1995, scanned with 30 μm (i.e. 0.3-m pixel size). Individual measurements below a certain value for the correlation coefficient were automatically deleted from the raw results. Displacement measurements pointing upslope (i.e. differing more than $\pm 90°$ from the local slope direction) were considered to be blunders and also eliminated automatically. Between 1976 and 1995, horizontal terrain shifts of altogether up to 2 m occurred. From measurements with higher temporal

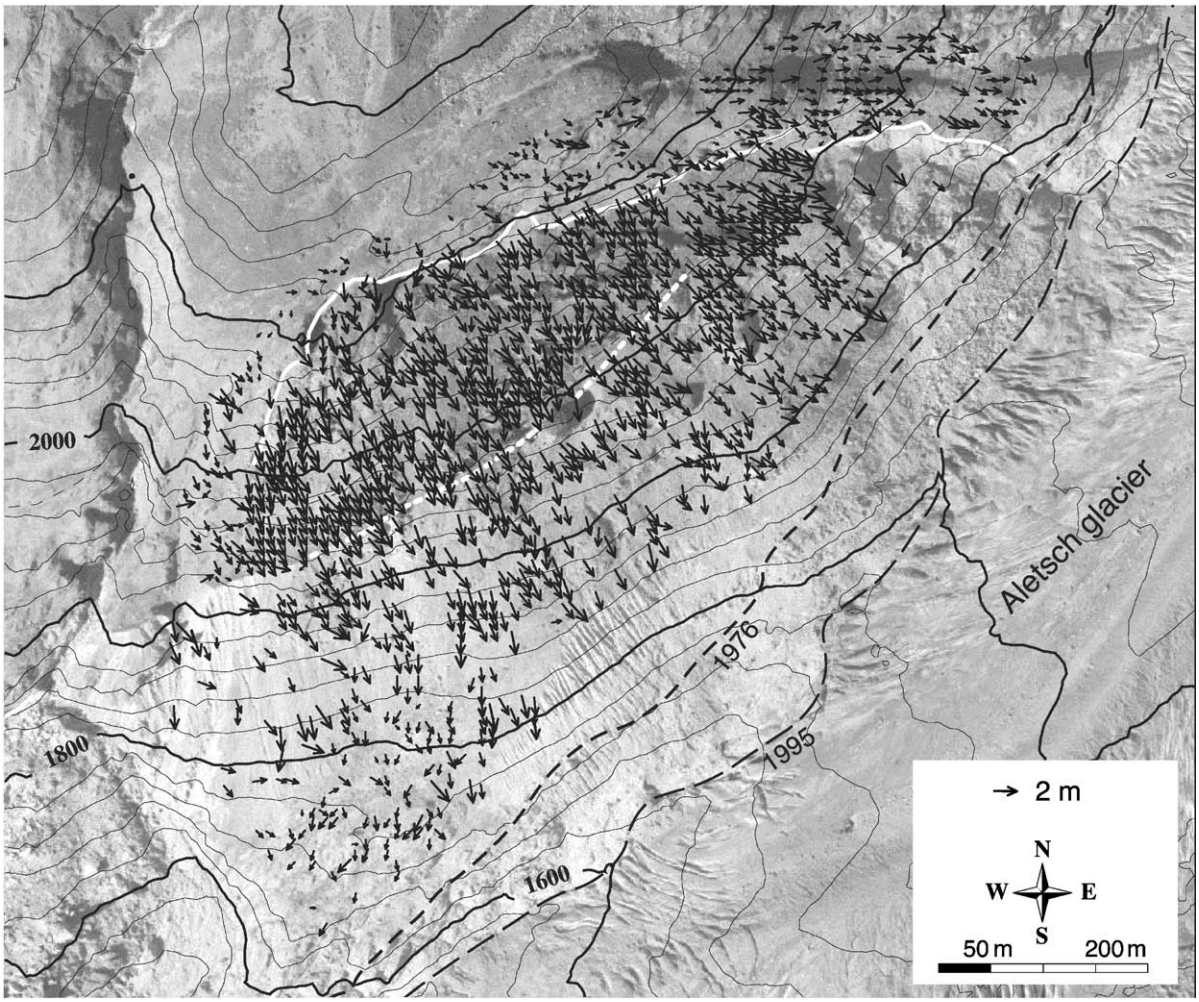

Fig. 6. Displacements on a rockslide near Aletsch glacier, Swiss Alps (8°01.5′E, 46°24.3′N) derived from orthoimages of 6 September 1976 and 2 October 1995. The solid white line to the North marks the upper edge of the slide; the dashed white line in the center marks the glacier moraine of 1850. To the southeast, the glacier boundaries of 1976 and 1995 are marked by dashed lines. Underlying orthoimage of 1995 based on aerial photography by the Swiss Federal Office of Topography. Maximum terrain deformation amounts to 2 m. The retreat of Aletsch glacier since the little ice age (ca. 1850) and the according loss of ice thickness by up to 300 m caused a stress-relief of the valley flank and related destabilization.

resolution (Kääb, 2000), we know that these displacements originate particularly from the second part of the observation period. Trigger of the rockslide is the retreat of the Aletsch glacier (lower right of Fig. 6) since the Little Ice Age (i.e. since approximately 1850), which caused a loss of glacier thickness of 200–300 m in the vicinity of the slide. The resultant lateral relief substantially changed the stress regime within the slope and, subsequently, destabilized it. A sharp increase of velocities marks the upper edge of the slide. Above the 1850 glacier moraine, displacement measurements were possible at most places. Below the 1850 moraine, places with corresponding surface features preserved over 1976–1995 were less dense due to surface erosion of morainic deposits. At the lower left of the unstable area, a change in the geology from the sliding schists to stable amphibolites can be observed. From the comparison of digitally

generated 1976 and 1995 DEMs, surface lowerings were found in the upper part of the slide, and corresponding uplifts in the lower part, both in similar order of magnitude as the horizontal shifts.

6. Conclusions and outlook

The presented case studies on glacier flow, permafrost creep and land sliding show that digital photogrammetric methods are highly suitable and efficient for monitoring high-mountain terrain deformation. (Note, that for technical reasons we applied aerial imagery scanned with 30 μm. Higher resolution would even improve the results.) Digital analysis of repeated optical imagery is able to contribute to the understanding of high-mountain mass transport and to assessing related hazards. As a rule of thumb, an accuracy for both horizontal and vertical changes of approximately one pixel sizes (RMS) can be expected. The factor most limiting this accuracy is often not the precision of the applied algorithms but the fuzzy nature of most high-mountain terrain features and extensive terrain changes over time. Especially the latter, however, are characteristic for mountain regions. For commercial applications, we consider the methods to be most promising for landslide monitoring. Thereby, the presented image analysis techniques, providing spatial coverage, are able to complement high-precision terrestrial deformation-measurements for selected points. Image analysis allows for reconstructing the deformation history, provided that suitable imagery is available.

However, some serious problems specific for high-mountain conditions (besides those specific to optical sensors in general) restrict the application of the presented methods. (1) Surface features with sufficient optical contrast must exceed the size of the image resolution and have to be preserved over the observation period. These requirements are often difficult to fulfil in high mountains owing to, for instance, ice and snow cover, ice and snow melt, frequent terrain destruction, or convection clouds. (2) The geometric changes might not exceed the significance level of the method applied. This problem occurs especially for rockslides, but applies in general for the use of comparably coarse image resolutions, such as the ASTER data. Therefore,

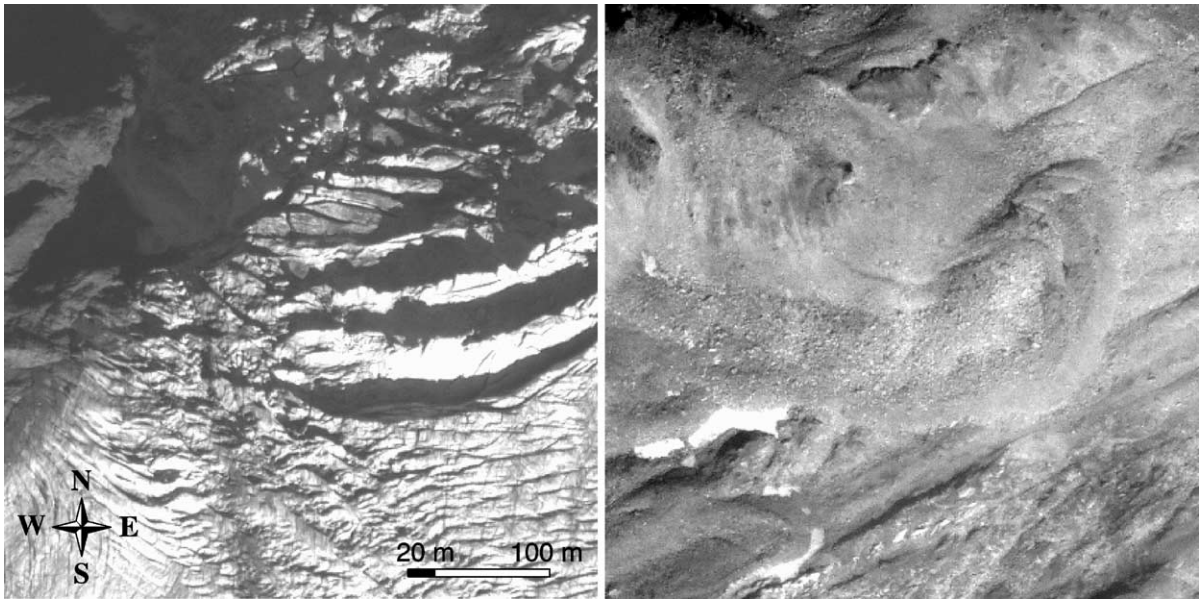

Fig. 7. Two sections of an IKONOS scene covering the Susten/Furka region, Swiss Alps (8°23′E, 46°38′N), showing Trift glacier (left) and a rock glacier near Furka pass (right). The accuracy for terrain-deformation measurements found from the presented case studies, on the one hand, and visual inspection of IKONOS scenes, on the other hand, indicate that terrain deformation could be measured from IKONOS imagery with roughly ±1–2 m RMS. IKONOS data of 17 September 2000 © Space Imaging Europe.

glacier thickness changes, usually in the order of m year^{-1}, or changes in rock glacier and landslide elevation can hardly be detected from repeated ASTER DEMs.

Potentially, two main image-acquisition parameters are available for meeting the above requirements: image resolution and time base between the acquisitions. New and upcoming optical sensors are especially improving these parameters by the following means. (1) The increasing number of available sensors or imagery, respectively, enhances the probability for finding suitable data. (2) The number of (satellite-) sensors dedicated for customer-controlled acquisition increases, as (3) their spatial resolution does. In that context, satellites like IKONOS or Quickbird are indeed able to bridge the gap between airborne and spaceborne optical sensors also for determining high-mountain terrain deformation. As a view on two sections of a high-mountain IKONOS scene shows (Fig. 7), enough details can be identified to expect an accuracy of 1–2 m RMS for measured terrain movements. This perspective might be especially interesting for monitoring glaciers and selected comparable fast rock glaciers in remote areas. However, in the near future the wide application of such high-resolution sensors for high-mountain research will be limited by the high data costs, the limited stereo availability, and the difficulty to obtain sufficiently accurate GCPs.

Acknowledgements

The work with ASTER data was started at the US Geological Survey in Flagstaff, AZ. Thanks are due to the Flagstaff GLIMS-team Hugh Kieffer, Jeff Kargel, Rick Wessels, Dave MacKinnon and others. The presented studies are partially financed by the Swiss National Science Foundation (21-54073.98, 21-59045.99). We also want to thank Rolf Hübscher, Hans-Peter Gautschi and Daniel Lüscher (Swiss Federal Office of Topography) for acquisition of the valuable aerial photographs. Sandra Eckert, Regula Frauenfelder, Christian Huggel, Tobias Kellenberger, Philippe Meuret, Frank Paul, Markus Vollmer, Bruno Weber and other staff and students of the Department of Geography, Zurich, provided support to the presented work. Special thanks are due to Armin Grün and Manos Baltsavias for their valuable comments on the manuscript.

References

Al-Rousan, N., Petrie, G., 1998. System calibration, geometric accuracy testing and validation of DEM and orthoimage data extracted from SPOT stereopairs using commercially available image processing systems. International Archives of Photogrammetry and Remote Sensing 34 (4), 8–15.

Baltsavias, E.P., Li, H., Stefanidis, A., Sinning, M., 1996. Automatic DSMs by digital photogrammetry. Surveying World 4 (2), 18–21.

Baltsavias, E.P., Favey, E., Bauder, A., Boesch, H., Pateraki, M., 2001. Digital surface modelling by airborne laser scanning and digital photogrammetry for glacier monitoring. Photogrammetric Record 17 (98), 243–273.

Baum, R.L., Messerich, J., Fleming, R.W., 1998. Surface deformation as a guide to kinematics and three-dimensional shape of slow-moving, clay-rich landslides, Honolulu, Hawaii. Environmental and Engineering Geoscience 4 (3), 283–306.

Blair, R.W., 1994. Moraine and valley wall collapse due to rapid deglaciation in Mount-Cook-National-Park, New Zealand. Mountain Research and Development 14 (4), 347–358.

Chandler, J.H., 2001. Terrain measurement using automated digital photogrammetry. In: Griffiths, J.S. (Ed.), Land Surface Evaluation for Engineering Practice. Geological Society of London, vol. 18, pp. 13–18.

Clague, J.J., Evans, S.C., 2000. A review of catastrophic drainage of moraine-dammed lakes in British Columbia. Quaternary Science Reviews 19 (17–18), 1763–1783.

ERSDAC, 1999a. ASTER User's Guide, Part I, Earth Remote Sensing Data Analysis Center, Tokyo, Japan. Available from http://www.science.aster.ersdac.or.jp.

ERSDAC, 1999b. ASTER User's Guide, Part II, Earth Remote Sensing Data Analysis Center, Tokyo, Japan. Available from http://www.science.aster.ersdac.or.jp.

Frauenfelder, R., Kääb, A., 2000. Towards a palaeoclimatic model of rock glacier formation in the Swiss Alps. Annals of Glaciology 31, 281–286.

Frezzotti, M., Capra, A., Vittuari, L., 1998. Comparison between glacier ice velocities inferred from GPS and sequential satellite images. Annals of Glaciology 27, 54–60.

Giani, G.P., Silvano, S., Zanon, G., 2001. Avalanche of 18 January 1997 on Brenva glacier, Mont Blanc Group, Western Italian Alps: an unusual process of formation. Annals of Glaciology 32, 333–338.

Haeberli, W., 1983. Frequency and characteristics of glacier floods in the Swiss Alps. Annals of Glaciology 4, 85–90.

Haeberli, W., Wegmann, M., Vonder Mühll, D., 1997. Slope stability problems related to glacier shrinkage and permafrost degradation in the Alps. Eclogae Geologicae Helveticae 90, 407–414.

Haeberli, W., Kääb, A., Wagner, S., Geissler, P., Haas, J.N., Glatzel-Mattheier, H., Wagenbach, D., Vonder Mühll, D., 1999. Pollen analysis and 14C-age of moss remains recovered from a permafrost core of the active rock glacier Murtèl/Corvatsch (Swiss

Alps): geomorphological and glaciological implications. Journal of Glaciology 45 (149), 1–8.

Haeberli, W., Kääb, A., Vonder Mühll, D., Teysseire, P., 2001. Prevention of debris flows from outbursts of periglacial lakes at Gruben, Valais, Swiss Alps. Journal of Glaciology 47 (156), 111–222.

Huggel, C., Kaeaeb, A., Haeberli, W., Teysseire, P., Paul, F., 2002. Remote sensing based assessment of hazards from glacier lake outbursts: a case study in the Swiss Alps. Canadian Geotechnical Journal 39, 316–330.

Kääb, A., 2000. Photogrammetry for early recognition of high mountain hazards: new techniques and applications. Physics and Chemistry of the Earth, Part B 25 (9), 765–770.

Kääb, A., 2001. Photogrammetric reconstruction of glacier mass balance using a kinematic ice-flow model: a 20-year time-series on Grubengletscher, Swiss Alps. Annals of Glaciology 31, 45–52.

Kääb, A., Funk, M., 1999. Modelling mass balance using photogrammetric and geophysical data. A pilot study at Gries glacier, Swiss Alps. Journal of Glaciology 45 (151), 575–583.

Kääb, A., Vollmer, M., 2000. Surface geometry, thickness changes and flow fields on permafrost streams: automatic extraction by digital image analysis. Permafrost and Periglacial Processes 11 (4), 315–326.

Kääb, A., Haeberli, W., Gudmundsson, G.H., 1997. Analysing the creep of mountain permafrost using high precision aerial photogrammetry: 25 years of monitoring Gruben rock glacier, Swiss Alps. Permafrost and Periglacial Processes 8 (4), 409–426.

Kääb, A., Gudmundsson, G.H., Hoelzle, M., 1998. Surface deformation of creeping mountain permafrost. Photogrammetric investigations on rock glacier Murtèl, Swiss Alps. Proc. 7th International Permafrost Conference, Yellowknife, Canada, pp. 531–537.

Kargel, J., 2000. New eyes in the sky measure glaciers and ice sheets. American Geophysical Union. EOS Transactions, 81 (24), 265, 270–271.

Kaufmann, V., Ladstädter, R., 2000. Spatio-temporal analysis of the dynamic behaviour of the Hochebenkar rock glaciers (Oetztal Alps, Austria) by means of digital photogrammetric methods. Proc. 6th International Symposium on High Mountain Remote Sensing Cartography, Ethiopia, Kenya, Tanzania (on CD-ROM).

Kirkbride, M., 1995. Ice flow vectors on the debris-mantled Tasman glacier, 1957–1986. Geografiska Annaler 77A (3), 147–157.

Kirkbride, M.P., Warren, C.R., 1999. Tasman glacier, New Zealand: 20th-century thinning and predicted calving retreat. Global and Planetary Change 22 (1–4), 11–28.

Lucchitta, B.K., Ferguson, H.M., 1986. Antarctica—measuring glacier velocity from satellite images. Science 234 (4780), 1105–1108.

Maas, H.G., Kersten, T., 1997. Aerotriangulation and DEM/orthophoto generation from high-resolution still-video imagery—on the potential of digital cameras onboard an aircraft. Photogrammetric Engineering and Remote Sensing 63 (9), 1079–1084.

Mantovani, F., Soeters, R., Van Westen, C.J., 1996. Remote sensing techniques for landslide studies and hazard zonation in Europe. Geomorphology 15 (3–4), 213–225.

Margreth, S., Funk, M., 1999. Hazard mapping for ice and combined snow/ice avalanches—two case studies from the Swiss and Italian Alps. Cold Regions Science and Technology 30 (1–3), 159–173.

McCarthy, J.J., Canziani, O.F., Leary, N.A., Dokken, D.J., White, K.S. (Eds.), 2001. Contribution of Working Group II to the Third Assessment Report of the Intergovernmental Panel on Climate Change (IPCC). Cambridge Univ. Press, UK.

Nakawo, M., Yabuki, H., Sakai, A., 1999. Characteristics of Khumbu Glacier, Nepal Himalaya: recent change in the debris-covered area. Annals of Glaciology 28, 118–122.

Powers, P.S., Chiarle, M., Savage, W.Z., 1996. A digital photogrammetric method for measuring horizontal surficial movements on the Slumgullion earthflow, Hinsdale county, Colorado. Computers and Geosciences 22 (6), 651–663.

Purdie, J., Fitzharris, B., 1999. Processes and rates of ice loss at the terminus of Tasman glacier, New Zealand. Global and Planetary Change 22 (1–4), 79–91.

Richardson, S.D., Reynolds, J.M., 2000. An overview of glacial hazards in the Himalayas. Quaternary International 65/66, 31–47.

Scambos, T.A., Dutkiewicz, M.J., Wilson, J.C., Bindschadler, R.A., 1992. Application of image cross-correlation to the measurement of glacier velocity using satellite image data. Remote Sensing of Environment 42 (3), 177–186.

Seko, K., Yakubi, H., Nakawo, M., Sakai, A., Kadota, T., Yamada, Y., 1998. Changing surface features of Khumbu glacier, Nepal Himalayas revealed by SPOT images. Bulletin of Glacier Research 16, 33–41.

Toutin, T., Cheng, P., 2001. DEM generation with ASTER stereo data. Earth Observation Magazine 10 (6), 10–13.

Van Puymbroeck, N., Michel, R., Binet, R., Avouac, J.P., Taboury, J., 2000. Measuring earthquakes from optical satellite images. Applied Optics 39 (20), 3486–3494.

Vollmer, M., 1999. Kriechender alpiner Permafrost: Digitale photogrammetrische Bewegungsmessung. Diploma thesis, Department of Geography, University of Zurich.

Weber, D., Herrmann, A., 2000. Contribution of digital photogrammetry in spatio-temporal knowledge of unstable slopes: the example of the Super-Saute landslide (Alpes-de-Haute-Provence, France). Bulletin de la Societe Geologique de France 171 (6), 637–648.

Würländer, R., Eder, K., 1998. Leistungsfähigkeit aktueller photogrammetrischer Auswertemethoden zum Aufbau eines digitalen Gletscherkatasters. Zeitschrift für Gletscherkunde und Glazialgeologie 34 (2), 167–185.

Zomer, R., Ustin, S., Ives, J., 2002. Using satellite remote sensing for DEM extraction in complex mountainous terrain: landscape analysis of the Makalu Barun National Park of eastern Nepal. International Journal of Remote Sensing 23 (1), 125–143.